Aerosol Science and Technology
Publication details, including instructions for authors and subscription information:
http://www.informaworld.com/smpp/title~content=t713656376

Experiments on the Low-Velocity Impact of Microspheres with Planar Surfaces

Patrick F. Dunn [a]; Raymond M. Brach [a];Michael J. Caylor [a]
[a] Particle Dynamics Laboratory, Department of Aerospace and Mechanical Engineering, University of Notre Dame, Notre Dame, IN

First published on: 01 January 1995

To cite this Article Dunn, Patrick F. , Brach, Raymond M. andCaylor, Michael J.(1995) 'Experiments on the Low-Velocity Impact of Microspheres with Planar Surfaces', Aerosol Science and Technology, 23: 1, 80 — 95, First published on: 01 January 1995 (iFirst)
To link to this Article: DOI: 10.1080/02786829508965296
URL: http://dx.doi.org/10.1080/02786829508965296

Experiments on the Low-Velocity Impact of Microspheres with Planar Surfaces

Patrick F. Dunn, Raymond M. Brach, and Michael J. Caylor
Particle Dynamics Laboratory,
Department of Aerospace and Mechanical Engineering,
University of Notre Dame, Notre Dame, IN 46556

Measurements of individual normal and oblique impacts of microspheres with planar surfaces are described and analyzed. Incident velocities from ~2 to 25 m/s and angles from 20° to 90° were controlled in the experiments for various combinations of microsphere and surface materials. For normal (90°) incidence, a single-component phase doppler particle analyzer system measured the incident and rebound normal velocities, particle diameter, and measurement volume crossing time. The resulting values of the kinematic coefficient of restitution revealed the effects of adhesion at lower incident velocities. In addition, the kinematic coefficient of restitution showed a direct dependency on surface material hardness. For oblique (< 90°) incidence, a pulsed laser light sheet visualization technique was used to determine the particle incident and rebound, normal and tangential velocity components. The resulting impulse ratio's variation with incidence angle helped delineate between rolling and sliding impacts. The sliding impact results in turn provided a measure of the coefficient of dynamic friction. All results were compared using the rigid body impact model of Brach and Dunn (1995), which includes the possibility of microsphere rotation. Subsidiary experiments also were performed to assess the effect of the charge transfer during individual impact events, and to search for evidence of plastic deformation resulting from impact.

INTRODUCTION

The impact of particles with surfaces has been studied for over 50 years. More recently, attention has focused on the impact of microparticles with surfaces and the role that adhesion plays in the process. For microspheres with diameters less than ~50 μm, impinging at velocities less than ~10 m/s, adhesion can significantly affect the rebound energy of the particle. To date, however, little direct experimental information has been gathered on the dynamic process of individual microparticle impacts. Normal impacts have been studied experimentally the most, and oblique impacts very little.

One of the earliest experiments in this area in which direct measurements of the pertinent parameters was reported by Dahneke (1975). He studied the normal impact of polystyrene latex microspheres (0.5–2.0 μm diameter) with target surfaces under vacuum conditions (~10^{-4} torr). In his experiments, the microsphere incident velocities ranged from ~2 to 35 m/s and were determined by measuring the time for the microspheres to pass through two parallel laser beams. Dahneke's data clearly illustrate the effect of particle adhesion at low incident velocities. Broom (1979) used high speed photography to measure the velocities of glass microspheres normally impacting various target surfaces. His work was restricted to very low incident velocities (0.1–0.5 m/s). Paw U (1983) also used a photographic technique in an interesting application-oriented study. His research was related

0278-6826/95/$9.50
SSDI 0278-6826(95)00002-W

Aerosol Science and Technology 23:80–95 (1995)

to vegetation pollenization by airborne particles; he used mostly natural materials for particles and surfaces. Buttle et al. (1989) used a modern laser doppler velocimeter system to measure incident and rebound velocities. Their work was restricted to a single, normal incident velocity (8.1 m/s) due to the fixed particle drop height in a vacuum. They used relatively large particles (48–107 μm diameter) which were less susceptible to adhesion effects.

One of the most comprehensive experimental investigations of small particle, normal impact was performed by Wall et al. (1990)[1]. In their experiments, ammonium fluorescein microspheres (3–7 μm diameter) were transported in an air jet at velocities ranging from $\sim$ 1 to 100 m/s to impact target surfaces made of four different materials. Their laser doppler velocity measurements were corrected for drag effects within the boundary layer. Ensemble averages of the incident and rebound velocities (as opposed to individual event measurements) were obtained and reported.

There have been less data gathered for the case of an oblique microparticle impact. Broom (1979) and Buttle et al. (1989) investigated glass particles obliquely impacting an aluminum target. Using his high speed photography technique, Broom examined impacts at 45 and 90° incidence.[2] Buttle et al. used a two-component laser Doppler velocimeter system to measure incident and rebound velocities for 29, 50 and 90° incidence.

A recent experimental study of microsphere impact with planar surfaces was conducted by Caylor (1993). Both normal and oblique impacts were investigated in which measurements were made during individual impact events. Microsphere incident velocity (from $\sim$ 2 to 25 m/s) and incidence angle (from 30 to 90°) were controlled. This paper describes the experimental techniques used by Caylor and presents some of his results and those of further experiments. The goals of this paper are (1) to describe experimental techniques that have been developed to successfully measure the key parameters that characterize individual microsphere/surface impact events, (2) to present the data acquired using polydisperse distributions of microspheres for both normal and oblique *individual* impact events, and (3) to compare the true mean value estimates of the data with the rigid model impact model of Brach and Dunn (1995).

EXPERIMENTAL SYSTEM AND APPROACH

An experimental system was developed specifically to investigate the impact of electrically "neutral" or charged ($\sim 10^{-16}$ to 10^{-14} C) microspheres ($\sim$ 1 to 75 μm diameter) with planar surfaces under vacuum conditions ($\sim 10^{-5}$ to 10^{-4} torr). A schematic of the experimental system with the configuration used for normal impact measurements is shown in Fig. 1. In the experiments, the microspheres, once ejected from a dispenser, were accelerated downward vertically over various distances by gravity to obtain the desired incident velocity of $\sim$ 2 to 25 m/s. Various particle and surface material combinations were examined. The target surface was oriented at various angles from 20° to 90° with respect to vertical such that either normal or oblique impacts could be studied. For the normal impact cases, a single-component phase doppler particle analyzer system was used to measure the incident and rebound normal velocity components, particle diameter and

[1]The results of this study are presented in more detail in an article by John (1995) in this special issue.

[2]Throughout this paper, the incidence angle is defined as the angle between the inbound particle trajectory and the surface, where 90° implies incidence normal to the surface.

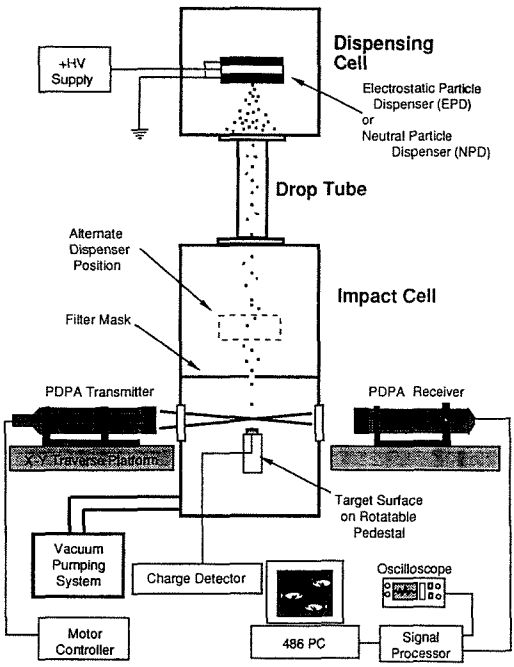

FIGURE 1. Schematic of the experimental configuration with the phase doppler particle analyzer system used in the normal impact experiments.

measurement volume crossing time. For the oblique cases, a pulsed laser light sheet visualization technique was used in conjunction with a video analysis system to determine the particle incident and rebound, normal and tangential velocity components. Subsidiary experiments also were performed to measure the charge transferred (from an electrically charged, conducting microsphere to an electrically grounded, conducting surface) or induced (by an electrically charged microsphere contacting the dielectrically coated surface of an electrically grounded conducting substrate) during impact, and to search for evidence of plastic deformation resulting from impact. The pertinent experimental subsystems will now be described further. The reader is referred to Caylor (1993) for a detailed description of the entire experimental system.

Particles and Impact Surfaces

Five surface and three particle materials were used and are presented in Tables 1 and 2, respectively, along with their important characteristics and material properties. The PDPA-measured diameter frequency distributions of the three types of microspheres are shown in Fig. 2. The Ag-coated glass microspheres were solid glass, covered by a ~ 500-Å-thick coating of Ag. Each of the metallic surfaces were machined from stock material into the shape of a Scanning Electron Microscope (SEM) specimen mount (1.27 cm diameter, 0.15 to 0.30 cm thickness). The stainless-steel, aluminum, and copper surfaces were hand polished using grit sizes from 6-μm diamond paste sequentially down to 0.05 μm colloidal silica particles to achieve smooth, mirror-like finishes. The targets were examined under an SEM to verify their surface quality. The stainless steel surface was virtually flawless to within the stated resolution of the instrument (40 Å). The surfaces made of softer materials (copper and aluminum) showed only few striations and irregularities, with dimensions on the order of a micron. After polishing, the surfaces were cleaned sequentially in baths of acetone, ethanol, and distilled water. They were blown dry with an N_2 jet and then baked at 200°C to evaporate any residual moisture. A stainless-steel surface was coated with a layer of Accuglass 110 Siloxane spin-on glass (SOG). The thickness of the glass coating was measured using an ellipsometer to be 2 μm. The Tedlar surface was prepared by bonding a piece of the 38 μm-thick film to a polished aluminum SEM mount using quick-setting epoxy. During an experiment, a target surface was mounted on a pedestal made of nylon that was attached to a three-axis micro-traverse.

TABLE 1. Characteristics of Microspheres Used in the Experiments

Surface Material[a]	Density (kg/m^3)	Yield Strength (MPa)	Young's Modulus (GPa)	Poisson's Ratio	Hertzian Stiffness (GPa)
Stainless steel	8000	310	190	0.27	73
Copper	8940	48	130	0.34	66
Aluminum	2700	21	69	0.33	51
Tedlar™	1460	N/A	2.1	0.33	3

[a] Values for the Siloxane-coated stainless steel surface were not available.

The metallic substrate of each pedestal was electrically grounded. The surface was aligned using a vertically positioned HeNe laser beam to within $\pm 1°$ of the desired impact angle.

Particle Charging and Dispensing System

The electrically conducting microspheres were dispensed under vacuum using an electrostatic particle dispenser (EPD). This device has been described by Olansen et al. (1989). Microspheres were charged by induction inside the EPD as they bounced toward its exit between conducting electrode plates maintained at different potentials. The charge and exit velocity of the microspheres are a function of the strength of the electric field within the EPD, which can be controlled. Resulting microsphere charges range from $\sim 10^{-16}$ to 10^{-13} C and exit velocities from ~ 0.1 to 20 m/s. Electrically "neutral" microspheres ($\sim 10^{-19}$ to 10^{-18} C) were dispensed using a neutral particle dispenser (NPD) operated in tandem with the EPD. Charged microspheres dispensed from the EPD were feed into the NPD and contacted its electrically grounded lower plate. The "neutral" microspheres were then dispensed from a hole in the bottom of the plate by mechanically vibrating the NPD's lower plate at ~ 10 Hz.

Phase Doppler Particle Analyzer (PDPA) System

A one-component PDPA system,[3] operated with frequency shifting and in the 30° forward scatter mode, was used to measure the normal components of the in-

[3]Aerometrics Model XMT-1100-5 transmitter, Model RCV-2100-5 receiver, 20 mW HeNe laser, 495 mm focal length lenses, 26.2 mm beam spacing, 1.52° interbeam half-angle, and 200 μm wide spatial filter slit.

TABLE 2. Properties of Materials Used for the Impact Surfaces

Microsphere Material	Nominal Diameter Range (μm)	Mean Diameter, d_{10} (μm)	Density (kg/m^3)	Young's Modulus (GPa)	Poisson's Ratio
Ag-coated Glass	1–30	8.6	2600	72	0.21
Stainless Steel10–65	49.9	8000	190	0.27	
Nickel	4–24	14.3	8850	200	0.31

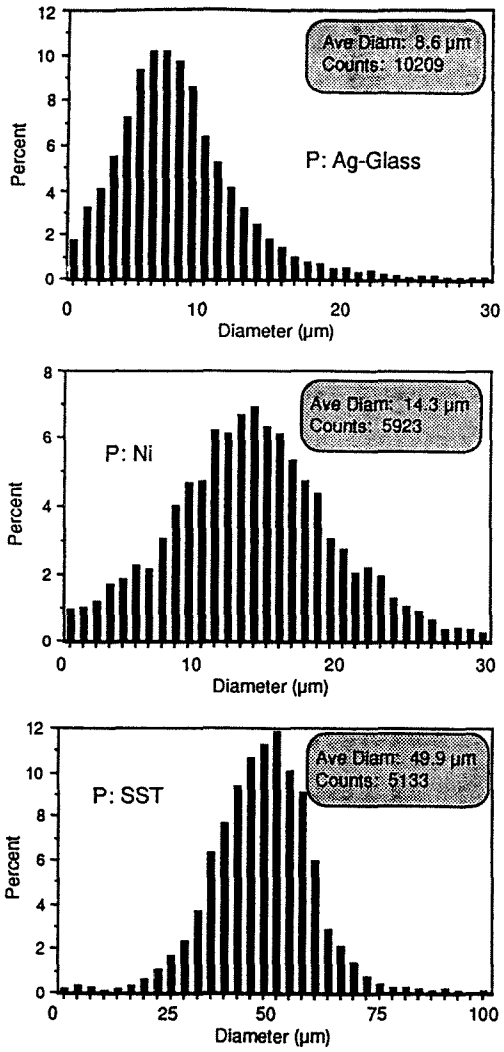

FIGURE 2. Diameter frequency distributions for the Ag-coated glass, nickel, and stainless-steel microspheres used in the subject experiments.

cident and rebound microsphere velocities. Its ellipsoidal measurement volume (~ 330 μm in diameter by 800 μm in length) was positioned to within 0.5 mm above the target surface. During an experiment, the raw PDPA data [the incident and rebound normal velocity component values, particle diameter and measurement volume crossing time] were stored in the system's 486 computer. Because particle impact occurred under vacuum conditions and the distance between the measurement volume and target surface was relatively small, the measured velocity component values were essentially those immediately before and after impact (see the discussion of measurement uncertainties later in this section). Various user-selectable velocity ranges (-3 to 3, -6 to 6, -12 to 12, and -25 to 25 m/s) were employed, depending upon the magnitude of the incident velocity. Resultant velocity component values were discretized into 200 bins over the chosen velocity measurement range. Customized data and reduction algorithms [described in detail by Caylor (1993)] were developed to match the incident normal velocity component with its appropriate rebound normal velocity component, thereby consolidating the information of an individual impact event. This was accomplished using the known measurement volume distance above the impact surface and the velocity component and time information. An example oscilloscope trace of a pair of doppler bursts obtained during a single microsphere/surface impact event is shown in Fig. 3. Velocity and diameter calibration checks of the PDPA system were performed during experiments using microspheres of known diameters that were accelerated by gravity over known distances under vacuum conditions. Estimates of the resultant uncertainties in the diameter and velocity component measurements are presented later in this section.

Particle Trajectory Imaging System (PTIS)

The pulsed laser light-sheet PTIS was used to study oblique impacts. A schematic of this system is shown in Figure 4. An argon ion laser beam (20–300 mW) was collimated and then directed through a spin-

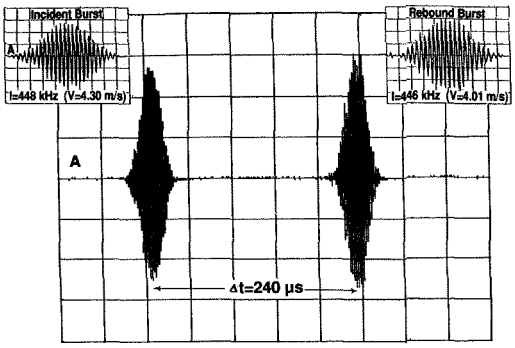

FIGURE 3. Digital oscilloscope recording of the doppler bursts generated during the incident and rebound phase of a single impact normal to a planar surface.

ning disk containing 10 evenly spaced slots. Depending on the angular velocity of the disk (measured with a digital stroboscope), strobe frequencies between ~ 50 and 1000 Hz were achieved. The chopped beam was directed through a plano-concave lens, which subsequently formed a pulsed light sheet aligned in a vertical plane above the target surface. Video images were acquired through a viewport located on the side of the vacuum chamber using a video camera and video cassette recorder. The camera was oriented normal to the light sheet. The image was enlarged as much as possible by using full zoom and by positioning the camera at the minimum focal distance (~ 1 m). This configuration yielded a field of view at the target impact plane of ~ 5 cm wide by 4 cm high. Based upon the frame rate, the field of view, and the strobe frequency, the system could measure microsphere velocities from ~ 0.1 to 30 m/s. Video data were acquired for various microsphere incidence angles for each particle/surface combination (typically at 20, 30, 45, 60, 75, and 90 degrees with respect to the target surface). An example image obtained by Caylor (1993) using this system is shown in Fig. 5. Estimates of the resultant uncertainties in the normal and tangential velocity components and the impact angles are presented later in this section.

Charge Measurement System

A charge measurement system was designed to measure the electrostatic charge transferred from an electrically charged microsphere to a conducting surface (or induced in an dielectric-coated conduct-

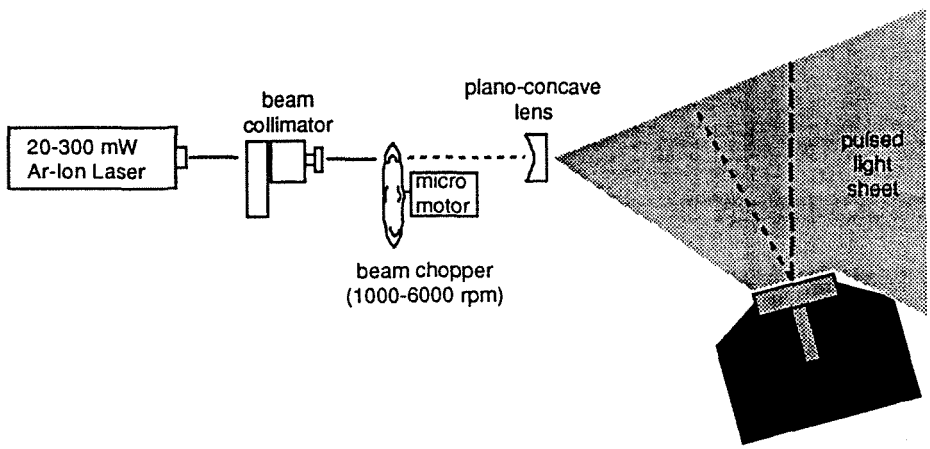

FIGURE 4. Schematic of the particle trajectory imaging system used in the oblique impact experiments.

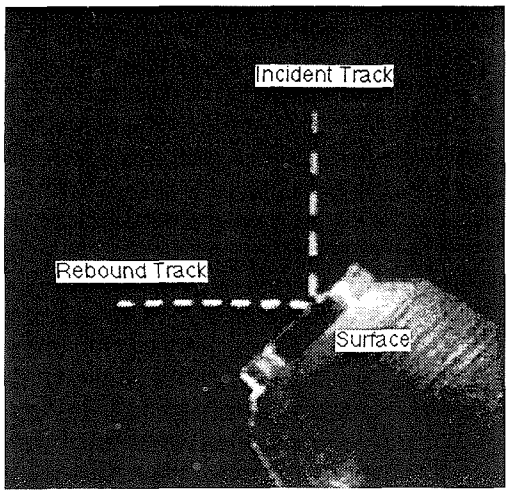

FIGURE 5. PTIS Image of a stainless-steel microsphere obliquely impacting a stainless-steel surface at incidence angle of 45°.

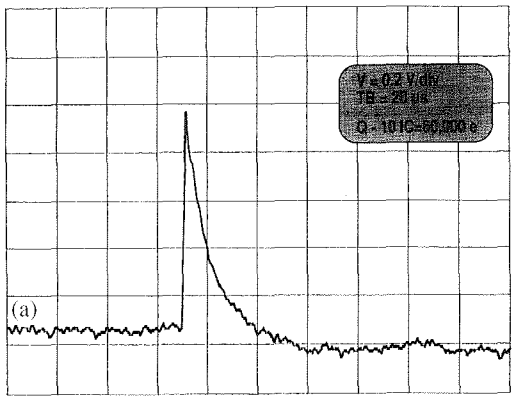

FIGURE 6. Digital oscilloscope recording of an image charge pulse from the charge measurement system of a Ag-coated glass microsphere impacting a Siloxane-coated copper surface.

ing surface) during impact [see Caylor (1993) for a detailed description]. During several subsidiary experiments, the charge was measured by charge sensitive preamplifier and shaping amplifier. The signal amplitude is linearly proportional to the magnitude of the input electrostatic charge (1.52 V/pC). Full amplitude was acquired within 2.5 μs and had a duration of ~ 10 μs. During an individual charge-transfer impact event, the output signal was stored on a digital oscilloscope; during multiple events, it was transferred in real-time to a multi-channel analyzer for subsequent analysis. A typical uncertainty in the charge measurement was determined from calibration to be $\sim \pm 3\%$[4]. For charges less than $\sim 4 \times 10^{-16}$ C, the uncertainties exceeded $\pm 10\%$ because of the inherent semiconductor noise. An example charge measurement system output for a Ag-coated glass microsphere impacting a Siloxane-coated stainless steel target surface is shown in Fig. 6.

[4]The uncertainty is ± 280 units of elementary charge (1e.c. $= 1.6 \times 10^{-19}$ C). This yields $\pm 3\%$ for 1.5×10^{-15} C and $\pm 10\%$ for 4×10^{-16} C.

Measurement Uncertainties

A standard uncertainty analysis at the 95% confidence level (Coleman and Steele 1989) was performed to estimate the uncertainties in the measured values of the microsphere's velocity components and impact angles, and in the resulting computed values of the coefficient of restitution and the impulse ratio.

For the normal impact experiments conducted using the PDPA system, uncertainties in the normal velocity component can arise primarily from (1) forces (gravitational, drag and electrostatic) acting on the microsphere between the measurement volume and the impact surface, (2) a quantization error introduced by the PDPA system software because of velocity discretization, and (3) the absolute uncertainty in the velocity component measurement. These three uncertainties were determined to be $\pm 0.1\%$, $\pm 2\%$ and $\pm 6\%$, respectively. These combined to yield overall uncertainties of $\pm 7\%$ and $\pm 10\%$

in the normal velocity component and the coefficient of restitution, respectively.

The elemental uncertainty in microsphere diameter measured using the PDPA system was determined through calibrations using either monodisperse polystyrene latex microspheres or an optical reticle (Caylor 1993) to range from $\pm 15\%$ at the smallest diameter (~ 2 μm) to $\pm 1\%$ at the largest diameter (~ 80 μm).

For the oblique impact experiments, the uncertainties for the normal and tangential velocity components and the incidence angles arise from the elemental uncertainties in measuring distances and angles as recorded on the digitized video images of the PTIS, and from the elemental uncertainty in the strobe frequency. These elemental uncertainties combine to yield uncertainties in the normal and tangential, incident and rebound velocity components that vary over the incidence angle range. Over the incidence angle range from 20° to 90°, the normal velocity component uncertainties decrease from $\pm 5\%$ to $\pm 1\%$ and the tangential velocity component uncertainties increase from $\pm 1\%$ to $\pm 8\%$. The resulting uncertainties in the coefficient of restitution and the impulse ratio are less than $\pm 8\%$ over the same range.

RESULTS AND DISCUSSION

Three types of microspheres and five different surfaces were used in the present normal impact experiments. For brevity, only some of the experimental results are presented and analyzed. The reader is referred to Caylor (1993) for more comprehensive results. Two particle/surface combinations, Ag-coated glass microspheres with stainless-steel and Tedlar surfaces, are presented in more detail. Comparatively, these two cases best illustrate the differences that occur between microsphere impact with a "hard" (high elastic modulus) surface versus "soft" (low elastic modulus) surface.

Normal Incidence (PDPA) Experiments: Experimental Results

Figure 7 displays the measured rebound-to-incident normal velocity component ratio (V_{nr}/v_{ni}) versus the incident velocity (v_{ni}) for Ag-coated glass microspheres impacting five different surfaces. Several observations are immediately apparent. For all five cases, the V_{nr}/v_{ni} ratios are relatively constant at the higher v_{ni}'s and decrease with decreasing v_{ni}. Below ~ 3 m/s, the V_{nr}/v_{ni} ratios decrease rapidly

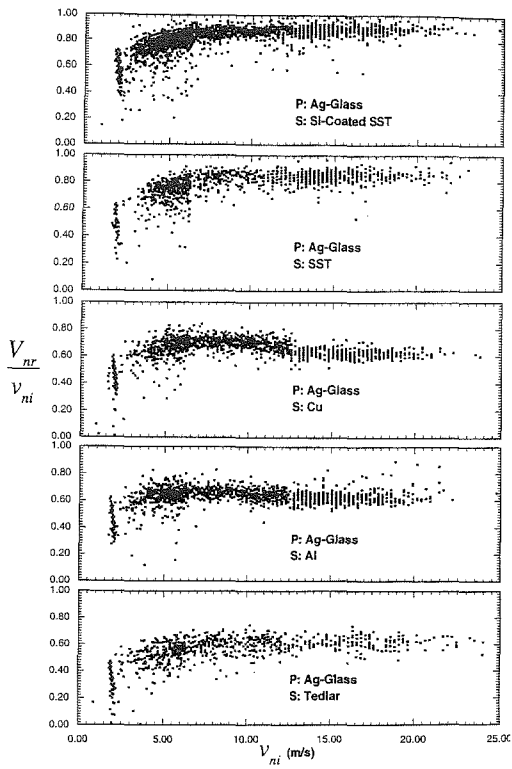

FIGURE 7. The rebound-to-incident normal velocity component ratio, V_{nr}/v_{ni}, versus the incident normal velocity component, v_{ni}, for the normal impact of Ag-coated glass microspheres with each of the five target surfaces.

toward zero values[5]. This trend is consistent with the results of previous investigators (e.g., Dahneke 1975; Wall et al. 1989), and serves to illustrate the increasing role of adhesion at lower velocities. Further, the V_{nr}/v_{ni} ratio values at the same initial velocity for the five surface materials are lowest for the lowest elastic modulus material (Tedlar) and increase with increasing elastic modulus of the material up to the highest cases (Siloxane-coated stainless steel and stainless steel). This illustrates that more energy is dissipated during impact with a softer surface, which results in a lower final velocity. Finally, variations occur in the measured V_{nr}/v_{ni} ratio values for a fixed v_{ni}. The causes for these variations are now discussed by considering an example case.

The sample mean values of the V_{nr}/v_{ni} ratio for v_{ni} increments of 1 m/s versus the initial velocity are shown in Fig. 8 for the Ag-coated glass microsphere/stainless-steel surface case. Each sample mean value is bounded by 95% confidence interval uncertainty bars. The bounds vary by approximately $\pm 10\%$ at the higher incident velocities and increase to approximately $\pm 35\%$–40% at lower v_{ni} values. Two of the factors that contribute to these variations include (1) the measurement uncertainty in the V_{nr}/v_{ni} ratio values resulting from the velocity measurement uncertainty itself, and (2) a "size" effect uncertainty that arises from the use of polydisperse microspheres. The "size" effect uncertainty occurs in the present experiments over the incident velocity range where the forces that contribute to adhesion are significant. Such forces are size

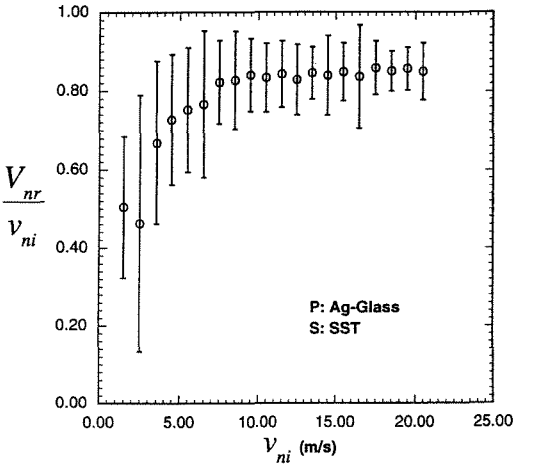

FIGURE 8. The sample mean values with 95% confidence limits of the rebound-to-incident normal velocity component ratio, V_{nr}/v_{ni} versus the incident normal velocity component, v_{ni}, for the normal impact of Ag-coated glass microspheres with a stainless-steel surface.

dependent (e.g., the van der Waals force). Ideally, this effect can be minimized by sorting the data with respect to size. However, the present data could not be presented in this manner because the resulting finite samples for a given initial velocity increment were not large enough to make statistically significant comparisons. At the higher v_{ni}'s (approximately ≥ 15 m/s) the observed variation is comparable to the measurement uncertainty resulting from velocity measurement uncertainty alone, and at the lower v_{ni}'s (≤ 15 m/s), to the measurement and "size" effect uncertainties combined in quadrature. Caylor (1993) has assessed the latter through modeling and has shown that it decreases from approximately $\pm 35\%$ at the lowest v_{ni} value to less than $\pm 1\%$ at v_{ni} values of approximately ≥ 15 m/s. Thus, the observed variations in the measured V_{nr}/v_{ni} ratio values for a fixed incident normal velocity are the result of velocity measurement and "size" effect uncertainties, where only the velocity

[5]The band of data at ~2 m/s is the result of a series of experiments in which the EPD was positioned closer to the target surface, thereby minimizing the free-fall distance. The discrete spacings between the data, particularly evident above ~12 m/s, result from the discretization of velocity by the PDPA system software.

measurement uncertainty predominates at the higher incident normal velocities. It is important to emphasize here that the observed variations are predominantly the result of the two uncertainties, and not the result of inherent variations from event to event (i.e., from "random" or uncontrolled variations during the experiment).

Normal Incidence (PDPA) Experiments: Model, Experimental Results Comparison

The rigid body impact model of Brach and Dunn (1995) is described in detail in a companion article in this special issue. Two different coefficients of restitution are considered in the model: the kinematic coefficient of resititution, e, which is the ratio V_{nr}/v_{ni}, and the kinetic coefficient of restitution, R, which is the ratio of the rebound-phase body-deformation impulse to the approach-phase body-deformation impulse, P_D^R/P_D^A. The latter coefficient involves the impulses due to only the internal dissipation of energy during impact (the deformation energy loss). The former also involves the energy expended by the microsphere during rebound against the forces[6] of adhesion in order to break contact with the surface (the adhesion energy loss). These coefficients appear in the conservation of energy equation for the microsphere:

$$(1-e^2)\left(\tfrac{1}{2}mv_{ni}^2\right) = (1-R^2)\left(\tfrac{1}{2}mv_{ni}^2\right) + W_A. \quad (1)$$

The term on the left-hand side of the equation is the total energy loss. The first term on the right-hand side is the energy lost due to dissipation and the second is the work required to overcome the forces of adhesion during rebound for the microsphere to leave the surface (the work of adhesion). Implicitly, the model assumes that there is no net overall potential energy gain or loss during impact, that energy losses due to adhesion occur only during the rebound-phase of contact, and that the processes of adhesion energy loss and deformation energy loss are independent.

A comparison of the experimental results for the cases shown in Fig. 7 with that model is presented in Fig. 9. In this figure, estimates of the true mean values of the V_{nr}/v_{ni} ratio are shown with 95% confidence limits for each 1 m/s v_{ni} increment. Presentation of data in this format provides for a proper statistical comparison with future experiments and also yields the appropriate values to which a theoretical model should be compared. The true mean value obtained from additional experiments performed under the same operating conditions will be within the ranges illustrated in the figure with 95% confidence (Coleman and Steele 1989). The bottom solid curves are the results of least squares fit of the data to the rigid body impact model expression for e and the top ones to the expression for R. The two coefficients of restitution are related to the adhesion coefficient, ρ (the ratio of the adhesion impulse to the body impulse during rebound), by the equation:

$$e = R[1-\rho]. \quad (2)$$

An arbitrary expression for the kinetic coefficient of restitution is chosen:

$$R = k/(k+v_{ni}), \quad (3)$$

in which k is an empirical constant. This functional form for R has been shown to successfully fit the data of Wall et al. (1990) (see Brach and Dunn 1992) and numerous other data (see Brach 1991).

[6]See Brach and Dunn (1992) for a summary of the forces that contribute to adhesion.

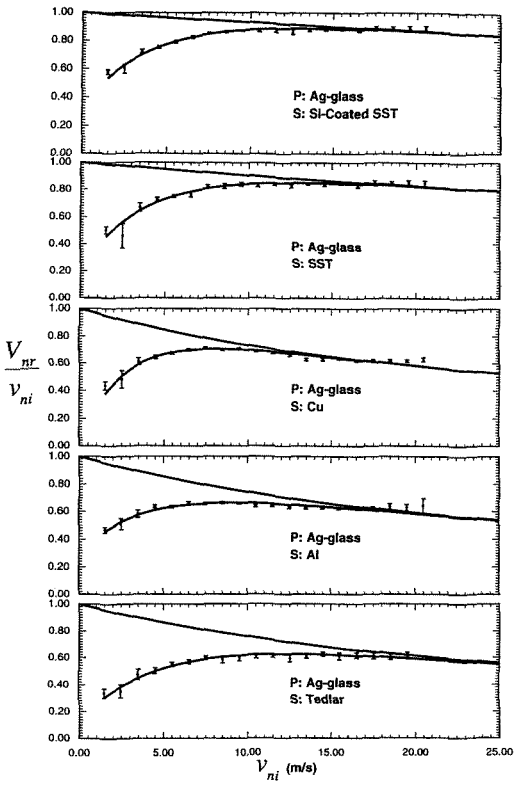

FIGURE 9. Estimates of the true mean values with 95% confidence limits of the rebound-to-incident normal velocity component ratio, V_{nr}/v_{ni}, versus the incident normal velocity component, v_{ni}, for the normal impact of Ag-coated glass microspheres with each of the five target surfaces compared with the rigid body impact model of Brach and Dunn (1995). For each target surface case, the top curve is R versus v_{ni}; the lower curve is e versus v_{ni}.

Another arbitrary expression for the adhesion coefficient is selected also:

$$\rho = b \exp\{-cv_{ni}\} \tag{4}$$

in which b and c are empirical constants. Only one least-squares fit is performed for each surface case by fitting the data to the equation:

$$e = [k/(k + v_{ni})][1 - b \exp\{-cv_{ni}\}], \tag{5}$$

yielding values for the constants k, b and c. The resultant values of the constants are presented in Table 3. As shown in the figure, the rigid body impact model fits the estimated true mean values of the data to within $\pm 2\%$ in almost all instances. Although the success of the model relies upon a curve-fit of the data to determine e, there are presently no models of the impact process that are based upon first principles only and do not resort to curve-fitting at some point. If a first-principles model for e were available, it could be incorporated readily into the present model.

By rearranging Eq. 1, it can be seen that the difference in the squares of the coefficients of restitution is related directly to the energy loss that occurs during impact due to adhesion. In particular, the rigid body impact model shows that:

$$e^2 - R^2 = W_A/[mv_{ni}^2/2], \tag{6}$$

in which the right hand side is the normalized work of adhesion, i.e., the work of the adhesion divided by the microsphere's incident kinetic energy. As described previously by Brach and Dunn (1992), when the kinematic and kinetic coefficients of restitution values are equal, the effects of adhesion are negligible. This is evident upon examining Eq. 2. The incident normal velocity component value at which this occurs in the mean, as seen in Fig. 9, is at approximately 15 m/s for the harder surface materials, and at approximately 20

TABLE 3. Values of Constants Obtained from a Least-Squares Fit of the Data to the Rigid Body Impact Model of Brach and Dunn (1995) for Each of the Five Target Surfaces

Surface Material	k	b	c
Siloxane-coated Stainless Steel	133.33	0.665	0.246
Stainless Steel	96.25	0.768	0.241
Copper	27.78	0.937	0.295
Aluminum	28.95	0.691	0.188
Tedlar™	31.37	0.858	0.153

m/s for the softest surface material, Tedlar. In this figure, in each plot, the top curve is R (as given by Eq. 3) versus v_{ni}; the bottom curve is e (as given by Eq. 5) versus v_{ni}.

Curves of the normalized work of adhesion versus the incident normal velocity are presented in Fig. 10 for each of the five surface materials. These results indicate for an incident normal velocity of 1.5 m/s that approximately 75% of the microsphere's incident kinetic energy is used to overcome the forces of adhesion in order for the microsphere to rebound away from the surface. This percentage decreases rapidly with increasing incident normal velocity up to 25 m/s, where it becomes less than 1%.

Oblique Incidence (PTIS) Experiments: Experimental Results

Three types of microspheres and four different surfaces were used in the present oblique impact experiments. Only the experimental results of Ag-coated glass microspheres impacting a stainless steel or a Tedlar surface are presented. These two cases illustrate best the differences that arise between microsphere impact with a "hard" versus "soft" surface.

For an oblique impact both normal and tangential velocity components can exist before and after impact, giving rise to normal and tangential impulses, P_n and P_t, over the duration of contact. The tangential mechanics of oblique impact is characterized using the coefficient $\mu = P_t/P_n$, the ratio of the tangential to normal impulses. For constant particle mass, the impulse ratio simply becomes the ratio of the difference between the initial and the final tangential (mass center) velocity components to the difference between the initial and the final normal (mass center) velocity components that arise from impact. That is, $\mu = (V_{tr} - v_{ti})/(V_{nr} - v_{ni})$. Kinematic conditions can

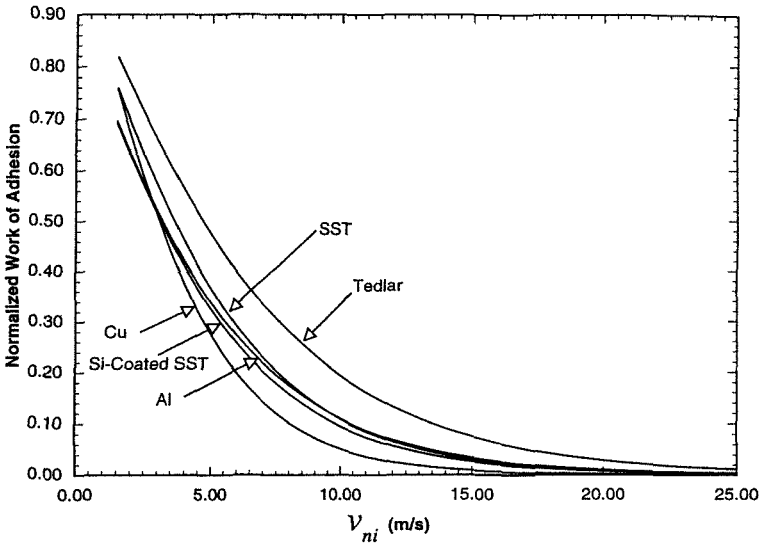

FIGURE 10. The work of adhesion normalized by incident kinetic energy as determined from the rigid body impact model of Brach and Dunn (1995) versus incident normal velocity for the normal impact of Ag-coated glass microspheres with each of the five target surfaces.

be used to place bounds on μ that demarcate sliding from rolling at separation (see Brach and Dunn 1995). Usually, the behavior of the impulse ratio is examined with respect to the particle's incidence angle, α, (the angle of the particle's incident velocity vector with respect to the surface, where $\alpha = 90°$ implies normal impact). Typically, at lower angles of incidence, the value of μ is constant because the microsphere slides along the surface throughout the duration of contact and, hence, upon release from the surface (see Brach 1991). For Coulomb friction, this constant value of μ is the dynamic friction coefficient. As the angle of incidence is increased further, the value of μ decreases because the microsphere is now rolling upon release from the surface (although the microsphere is sliding at the time of initial contact). Rolling occurs during the period of contact when the relative tangential velocity between the microsphere and the surface becomes zero. The angle of incidence at which the microsphere is rolling (instead of sliding) upon release from the surface is termed the critical angle of incidence. Eventually, upon reaching $\alpha = 90°$, the value of μ becomes zero because there is no tangential impulse if there is no initial angular velocity.

The impulse ratio versus incidence angle data is shown in Fig. 11 for the cases of Ag-coated glass microspheres obliquely impacting either a stainless-steel or a Tedlar surface. The mean values are connected by straight lines. For the stainless-steel surface case, the mean values of μ are constant (within the experimental uncertainty) from 18° to 60°, and then decrease up to 90°. This implies that on the average the microspheres slide throughout contact between 18° and 60° and roll upon separation from the surface between 60° and 90°. This implies that the critical angle of incidence for this case is 60°. The case of the Tedlar surface is somewhat

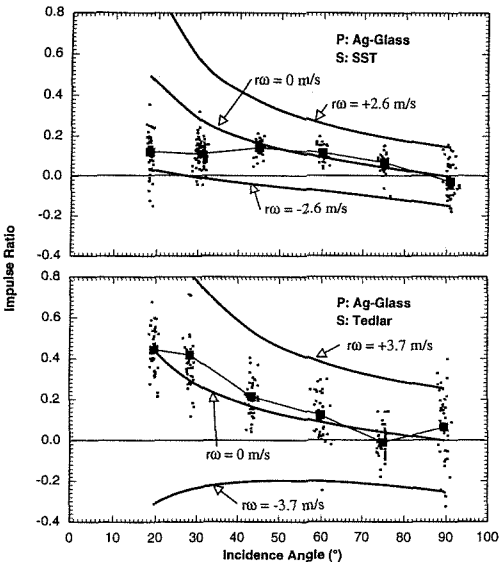

FIGURE 11. The impulse ratio versus the incidence angle for the cases of AG-coated glass microspheres obliquely impacting either a stainless-steel or a Tedlar surface.

different, where, in general, the mean values of μ continue to decrease with increasing incidence angle. Comparatively, the softer Tedlar surface induces rolling upon separation over a much broader range of incidence angles than the harder stainless steel surface does. This implies a higher dynamic coefficient of friction between Ag-coated glass microspheres and Tedlar versus stainless steel. For the Tedlar surface case, the critical angle of incidence is approximately 20°.

The variations in μ at a fixed angle of incidence are the direct result of the variation in rebound angle. In the present experiments, the typical variation in rebound angle for a given angle of incidence was approximately $\pm 5°$. This variation was similar when either relatively polydisperse (e.g., 1–30 μm diameter Ag-coated glass) or relatively monodisperse (e.g., 64–76 μm diameter stainless steel) microspheres impacted against the same surface. This rebound angle spread is assumed to be pre-

dominantly result of the microspheres having different rotational velocities when they impact the surface at a given angle of incidence. Thus, the observed variations in μ are the result of variations in microsphere rotation prior to impact (to within the measurement uncertainty in μ which was estimated to be $\pm 8\%$) and not the result of inherent variations from event to event (i.e., from "random" or uncontrolled variations during the experiment).

Also shown for each of the cases in Fig. 11 are two solid curves that represent the $+r\omega$ (counter-clockwise, forespin) and $-r\omega$ (clockwise, backspin) initial rotational velocity range calculated from the rigid body impact mechanics model of Brach and Dunn (1995) *assuming rolling upon separation from the surface*. An additional solid curve is presented for zero initial rotational velocity ($\omega = 0$).[7] The specific limiting $r\omega$ values are obtained using the maximum experimental value of μ found from the 90° case (where the incident tangential velocity component value is negligible with respect to the rotational velocity). The limiting curves are then calculated from the model over the incidence angle range assuming a constant value of $r\omega$ and using the mean values of kinematic coefficient of restitution and incident normal velocity component found from the 90° case. Both positive and negative rotational velocity values can be present because of the symmetric geometry of the particle dispenser. A negative value of μ can arise, for example, from the impact of a microsphere having initial backspin. This is because for this case the rebound tangential velocity component is smaller than the incident tangential velocity component.

Individual values of the measured rebound-to-incident normal velocity component ratio (V_{nr}/v_{ni}) versus the initial normal velocity component (v_{ni}) are displayed in Figure 12 for the oblique impact data that were presented in Figure 11. As can be seen in the figure, there is no average trend of decreasing V_{nr}/v_{ni} values with decreasing v_{ni} values as was seen for the same microsphere/surface combinations and v_{ni} values studied in the normal incidence impact experiments (see Fig. 7). The means and the standard deviations of the rebound-to-incident normal velocity component ratios are 0.74 and 0.18, and 0.67 and 0.23 for the stainless steel and Tedlar surfaces, respectively. The Tedlar case has a lower mean value,

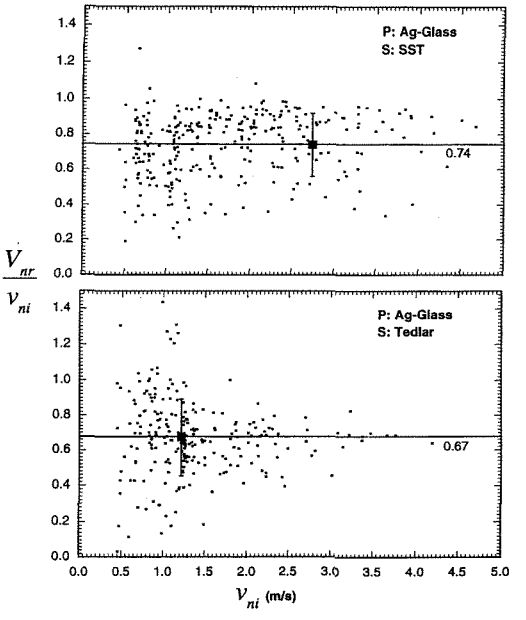

FIGURE 12. The rebound-to-incident normal velocity component ratio, V_{nr}/v_{ni}, versus the incident normal velocity component, v_{ni}, for the cases of Ag-coated glass microspheres obliquely impacting either a stainless-steel or a Tedlar surface.

[7]For all angles of incidence between the critical angle of incidence and 90°, a microsphere with no rotational velocity will roll upon release from the surface. However, at exactly 90° incidence, a perfectly round, non-rotating microsphere impacting a perfectly smooth surface will neither roll nor slide.

as expected for the softer surface case. Clearly, other factors such as microsphere rotation prior to impact can confound the interpretation of oblique impact data when viewed in this simple manner.

Subsidiary Experiments

Additional experiments were performed to experimentally determine whether or not the level of microsphere charge (from $\sim 10^{-16}$ to 10^{-14} C per microsphere) was sufficient in the present experiments to affect the values of the kinematic coefficient of restitution. Ag-coated glass microspheres, both electrically "neutral" and charged to the aforementioned levels, were impacted in separate experiments against a Siloxane-coated stainless steel surface, giving rise to the highest possible magnitude in the electrostatic image force in the present experiments. The results revealed no difference (to well within the measurement uncertainty) between the two cases, supporting the calculations of Caylor (1993), which showed that charge levels of $\sim 10^{-13}$ C or greater are required for this case before electrostatic forces become significant.

Other subsidiary experiments were conducted to examine if plastic deformation could occur from impact for the types of materials and conditions of the present experiments. Conclusive, visual evidence of plastic deformation was sought using scanning electron microscopy of the microspheres and target surfaces. Two types of relatively "hard" microspheres (Ag-coated glass and 60-125 μm diameter stainless steel) were impacted against different impact zones on a relatively "soft," highly polished, aluminum target surface. The average values of the incident kinetic energy per microsphere were 0.05 and 20 nJ for the Ag-coated glass and 60–125-μm-diameter stainless-steel microspheres, respectively. No visual evidence of plastic deformation was found for the Ag-coated glass microsphere case. A few indentations (~ 10 μm in diameter) were observed in the aluminum surface for the stainless steel microsphere case (see Caylor, 1993, for micrographs of the surface). Thus, for the experimental results reported herein, in which the incident kinetic energies per microsphere were less than 0.2 nJ, it is highly unlikely that plastic deformation of the surface material occurred. Yet, it is possible that plastic deformation can occur in microsphere impact experiments. For example, Wall et al. (1990), using "soft" ammonium fluorescein microspheres and extending their impacts to much higher velocities (as compared with the relatively "hard" microspheres and lower velocities examined in the present study), attributed plastic damage to the microspheres and not to the surface. It is important to note, however, that no conclusive visual evidence of plastic deformation on either particles or surfaces has ever been presented in the open literature for the case of microparticle impact. One possible argument against the occurrence of plastic deformation in the present and other similar experiments, that the yield limit may not be exceeded at typical microparticle impact strain rates, has been offered by Brach (1993). He noted that the strain rates encountered in typical microparticle impact experiments ($\sim 10^6$/s) are at least 3 orders of magnitude higher than most measures of "high" strain rate yielding of common materials (Meyers et al., 1992). Furthermore it is known that as strain rates increase, a ductile material's yield strength approaches an increasing ultimate strength and the material becomes stronger but more brittle. This information supports that plastic deformation may not necessarily occur under typical microsphere impact conditions, as evidenced by the lack of visual observation in the present study.

SUMMARY AND CONCLUSIONS

The results of experiments on the individual impacts of microspheres under either normal or oblique incidence with planar surfaces were presented. The features of two unique experimental systems designed to study normal and oblique microsphere impacts under vacuum conditions were described.

The normal impact data acquired clearly illustrated the effects of adhesive forces and surface material hardness on the kinematic coefficient of restitution, particularly at the lower incident velocities. Application of the rigid body impact model of Brach and Dunn (1995) to the data revealed the range of incident normal velocities over which adhesion effects were present. The model was used further to show that at lower incident velocities a significant portion of the microsphere's incident kinetic energy was used to overcome the forces of adhesion in order to achieve microsphere rebound from the surface.

The oblique impact data established the incidence angle ranges over which microsphere rotation upon separation from the surface and sliding throughout the duration of surface contact occurred. However, no effects marking the presence of adhesive forces were discernible by sole examination of the kinematic coefficient of restitution, which was found to be independent of the incident normal velocity component. The rigid body impact model also was used to assess the effects of microsphere rotation on rolling versus sliding.

Finally, the results of subsidiary experiments supported the absence of both charge effects and plastic deformation in the present experiments.

In conclusion, this study has demonstrated that the key parameters characterizing *individual* microsphere/surface impact events can be measured for both normal and oblique microsphere impacts with planar surfaces under vacuum conditions and that a rigid body impact model can be applied to the data to reveal more subtle effects present in the experiments.

We acknowledge the support of M. J. Caylor by the United States Air Force during the course of his doctoral research, the University of Notre Dame's Jesse Jones Research Grant (#2420-45462) and the Sigma XI Research Society for partial equipment support, Dr. Keng Leong of Argonne National Laboratory for the loan of the PDPA system, Mr. Greg Janson for acquiring further oblique impact data, and Mr. Jonathan Fay for data reduction and plotting. Finally, we wish to acknowledge funding from the Electric Power Research Institute (RP8034-03, Dr. Richard Oehlberg, Project Manager), which has supported part of the present study and has allowed us to continue this research.

REFERENCES

Brach, R. M. (1991). *Mechanical Impact Dynamics*, Wiley, New York.

Brach, R. M., and Dunn, P. F. (1992). *Aerosol Sci. Technol.* 15:51–64.

Brach, R. M. (1993). *Proceedings of the 1993 Annual Meeting of The American Association for Aerosol Research*, Oak Brook, IL.

Brach, R. M., and Dunn, P. F. (1995). *Aerosol Sci. Technol.* 23:51–71.

Broom, G. P., 1979. *Filtration Separation* 16:661–669.

Buttle, D. J., Martin, S. R., and Scruby, C. B., 1989. Harwell Laboratory Report AERE-R13711, Oxfordshire, UK, 1–30.

Caylor, M. J., 1993. Ph.D. dissertation, University of Notre Dame, Notre Dame, IN, USA.

Coleman, H. W., and Steele, W. G. (1989). *Experimentation and Uncertainty Analysis for Engineers*, Wiley, New York.

Dahneke, B., 1975. *J. Colloid Interface Sci.* 51:58–65.

John, W., 1995. *Aerosol Sci. Technol.* 23:2–24.

Meyers, M. A., Murr, L. E., and Staudhammer, K. P., 1992. *Shock-Wave and High-Strain-Rate Phenomena in Materials*, Marcel Decker, New York.

Olansen, J. B., Dunn, P. F., and Novick, V. J., 1989. *J. Appl. Phys.* 66:6098–6109.

Paw U, K. T., 1983. *J. Colloid Interface Sci.*, 93:442–452.

Wall, S., John, W., Wang, H-C., and Goren, S. L. 1990. *Aerosol Sci. Technol.* 12:926–946.

Received August 1, 1994; revised January 4, 1995